Temporal association in neural networks at finite temperatures

M. Y. Choi, Jihyun Choi,* and Kibeom Park
Department of Physics and Center for Theoretical Physics, Seoul National University, Seoul 151-742, Korea
(Received 6 July 1998)

Temporal association in neural networks, which retrieves time sequences of stored patterns, is made possible by introducing asymmetry in the synaptic coupling. Such temporal association in the asymmetric Hopfield model is first considered, with particular attention to the finite-temperature effects on the retrieval capability. We then turn to the dynamic model, which is the main topic of this paper, and investigate its temporal association properties both analytically and numerically. The phase diagram is obtained in the three-dimensional parameter space, and its structure is discussed according to the storage and other parameter values. [S1063-651X(98)10212-X]

PACS number(s): 87.10.+e, 64.60.Cn, 89.70.+c

I. INTRODUCTION

The study of the thermodynamic properties of neural networks has focused mostly on the systems with symmetric couplings [1–3], which makes the dynamics of the network relatively simple. The system relaxes to the states which are local minima of a global energy function and remains stable at low temperatures. Thus symmetric networks cannot provide *temporal association*, which retrieves a sequence of embedded patterns successively. Such a capability of recalling temporal sequences or cycles of patterns can be endowed by introducing asymmetric couplings in the network, which may prevent the system from approaching a stable attractor in the configurational space [4–8]. Note that the synaptic connections in real biological systems indeed have a high degree of asymmetry. It is also natural to allow time delay in the asymmetric part of the synaptic coupling [9]: It is desirable to have a controlled set of transitions in such a way that the system stays in one state for a finite period of time after which a transition is made to the next quasiequilibrium state in the sequence. Without the time delay, the system would make transitions among quasiequilibrium states at once.

In the Hopfield-type neural networks, the desired features of temporal association have been successfully demonstrated with the asymmetric coupling [4]; the important role played by the transmission delay has also been observed. However, the study is restricted to the low-loading and zero-temperature limit, and the behavior at finite storage and finite temperatures has not been investigated. Furthermore, the totally asynchronous character of the dynamics in the Hopfield model does not describe the real biological situation very well. On the other hand, the dynamic model proposed by one of us [10] deals with usual continuous time rather than digital and takes into account the existence of relevant time scales in the nervous system such as the refractory period, time duration of the action potential, and retardation of the signal propagation. In particular, the dynamic model possesses time delay inherently, and is apparently adequate for studying temporal association.

In this paper, we study both analytically and numerically temporal association in the Hopfield model and in the dynamic model, with emphasis on the effects of finite storage and temperatures. In the Hopfield model the phase diagram is obtained in the plane of the temperature and the degree of asymmetry, for various storage values. The dynamic model is also made capable of temporal association by introducing asymmetric couplings in a similar way to the Hopfield model. In addition to the temperature and the degree of asymmetry, there exists one more parameter of relevance in the dynamic model—the ratio of the refractory period to the action potential duration. The corresponding phase diagram in the three-dimensional parameter space is obtained via stability analysis and compared with the results of numerical simulations.

This paper is organized as follows. In Sec. II, we introduce temporal association in the asymmetric Hopfield model and study numerically its properties at finite temperatures and finite storage capacity. The phase diagram is obtained in the plane of the temperature and the degree of asymmetry. Section III is devoted to the investigation of the temporal association in the dynamic model, presenting the main results of this paper. We first derive analytic phase boundaries by means of stability analysis, and also perform numerical simulations to obtain the phase diagram. The two phase diagrams, obtained via stability analysis and from numerical simulations, are drawn in the three-dimensional parameter space, and found to display good agreement with each other. Finally, a brief summary is given in Sec. IV.

II. ASYMMETRIC HOPFIELD MODEL

We follow Ref. [4] and consider a network of N two-state neurons, where the state of the ith neuron is described by the variable $s_i(=\pm 1)$. Temporal association is accomplished by introducing two kinds of synaptic couplings as well as a time constant τ characterizing the dynamic memory. Synapses of the first kind are symmetric, given by Hebb's rule

$$J_{ij}^{S}=\frac{1}{N}\sum_{\mu=1}^{p}\xi_i^{\mu}\xi_j^{\mu} \quad (i\neq j) \tag{1}$$

for p stored patterns $\{\xi_i^{\mu}\}$, as in the standard Hopfield model; those of the second kind are asymmetric, taken in the form

*Present address: Brain Research Center, Pohang University of Science and Technology, Pohang 790-784, Korea.

$$J_{ij}^{A}=\frac{\lambda}{N}\sum_{\mu=1}^{q}\xi_i^{\mu+1}\xi_j^{\mu}\quad(i\neq j),\tag{2}$$

which defines the order among the $q(\leqslant p)$ patterns. The relative strength λ of the asymmetric part controls the degree of asymmetry, and cycles can be incorporated by setting $\xi_i^{q+1}=\xi_i^1$ in Eq. (2). At zero temperature, i.e., in the absence of stochastic noise, the system evolves in time as follows: The state of the (randomly chosen) ith neuron is updated in such a way that s_i has the same sign as the local field $h_i\equiv\Sigma_j J_{ij}s_j$. The local field consists of the two contributions,

$$h_i=\sum_{j=1}^{N}J_{ij}^{S}s_j+\sum_{j=1}^{N}J_{ij}^{A}\overline{s_j}\tag{3}$$

with

$$\overline{s_j}\equiv\int_0^t dt' w_\tau(t-t')s_j',$$

where s_j' represents the state of the jth neuron at time t'. Here $w_\tau(t)$ denotes the dynamic memory characterized by the time-delay constant τ. It is non-negative and normalized to be $\int_0^\infty dt w_\tau(t)=1$. The effects of noise can be taken into account by updating the ith neuron probabilistically. Namely, the value $s_i=+1$ is assigned according to the probability $2^{-1}(1+\tanh\beta h_i)$, where the ''temperature'' $T\equiv\beta^{-1}$ measures the noise strength [2]; this is essentially the standard Monte Carlo process.

The analysis of the emergent dynamic features of the network becomes particularly simple in the limit $N\to\infty$ with finite p. In this zero-storage case ($\alpha\equiv p/N\to 0$) the local field takes the form

$$h_i=\sum_{\nu=1}^{p}\xi_i^{\nu}m_\nu+\lambda\sum_{\nu=1}^{q}\xi_i^{\nu+1}\overline{m}_\nu,\tag{4}$$

where m_ν is the overlap with the νth pattern and $\overline{m}_\nu$ is the time average of m_ν:

$$m_\nu\equiv N^{-1}\sum_{i=1}^{N}\xi_i^{\nu}s_i,$$

$$\overline{m}_\nu\equiv\int_0^t dt' w_\tau(t-t')m_\nu'$$

with m_ν' being the overlap at time t'. The overlap of the order unity, $m_\mu\approx 1$, which implies that the state of the network is strongly correlated with one of the embedded patterns (i.e., with the μth one), describes the state with stationary memory. On the other hand, in the state without memory all the average overlaps are inappreciable and of the order of $N^{-1/2}$. Thus the no-memory state is characterized by $m_\nu\approx 0$ for all ν $(=1,\ldots,p)$, implying that the system is not correlated with any embedded pattern.

At zero temperature it has been shown that the system which initially learns the first embedded pattern might transit to the second one after a finite-time duration t_0 if λ exceeds a certain critical value λ_c [4]. The transition occurs successively to the next pattern after t_0 and finally constitutes a cycle of temporal association. The time interval t_0 and the critical value λ_c depend on the specific form of the memory function $w_\tau(t)$. Here, for convenience, we consider the simple case $w_\tau(t)=\delta(t-\tau)$, which is expected to display temporal association for all values of λ larger than λ_c [4,6]. As the storage α is increased from zero, fluctuations in the local fields produced by nonzero α has been suggested to induce transitions even for smaller λ, thus lowering the critical value λ_c. At high temperatures, on the other hand, large fluctuations tend to mix the patterns and to yield random overlaps among the patterns, which deteriorates the capability of the network to recall the proper patterns. Accordingly, temporal association is suppressed and the critical value λ_c is expected to increase with α.

To investigate these properties in detail, we have performed numerical simulations of the system at various temperatures and storage values. The behavior of the overlap m_ν obtained from the simulations of the system with $N=1000$ and $p=q=10$ is displayed in Fig. 1. At zero temperature ($T=0$) the characteristics of temporal association are shown in Figs. 1(a) and 1(b): When λ is less than λ_c (≈ 0.78 for $\alpha=0.01$) [11], the system stays in the initial pattern $\xi^{\nu=1}$ indefinitely, yielding a stationary state, while for $\lambda>\lambda_c$, transitions to the next patterns occur successively with the time interval t_0 equal to τ. At nonzero but low temperatures, the state determined by the local fields $\{h_i\}$ for $0<t<\tau$ will have an overlap with the pattern $\xi^{\nu=1}$ less than unity and nonzero overlaps with other patterns, i.e., $m_\nu\neq 0$ even for $\nu\neq 1$. Accordingly, small fluctuations tend to induce the transition even at the value of λ less than unity, as shown in Figs. 1(c) and 1(d). In other words, the critical value λ_c in general decreases as the temperature T is raised from zero. At higher temperatures, however, all the overlaps display large fluctuations [compare Fig. 1(e) with Fig. 1(c)]. Such large fluctuations suppress temporal association in the system, making it necessary to have a large value of λ for temporal association. It is thus concluded that the critical value λ_c at first decreases with temperature but eventually increases as the temperature is raised further.

To determine the phase boundaries between the state with stationary memory such as (c) and that with temporal association such as (d), we use the following criterion: The system is considered to have stationary memory if the memory of a single pattern is dominant during the simulation time, i.e., if $I_\mu>\Sigma_{\nu\neq\mu}I_\nu$. Here I_μ is the number of time steps in the simulation during which m_μ is the maximum. Similarly, the fluctuating state without memory is distinguished according to whether the maximum overlap is smaller than the sum of the next two overlaps during more than half the simulation time.

Figure 2 presents the schematic phase boundaries in the λ-T plane, separating the stationary-memory state (SM), the temporal-association state (TA), and the no-memory state (NM), for several values of α. For small values of λ and α, the system displays stationary memory of a single pattern at low temperatures. As the temperature T is raised, however, overlaps with other patterns become increased, inducing transitions into other patterns. Accordingly, the system displays temporal association. At even higher temperatures,

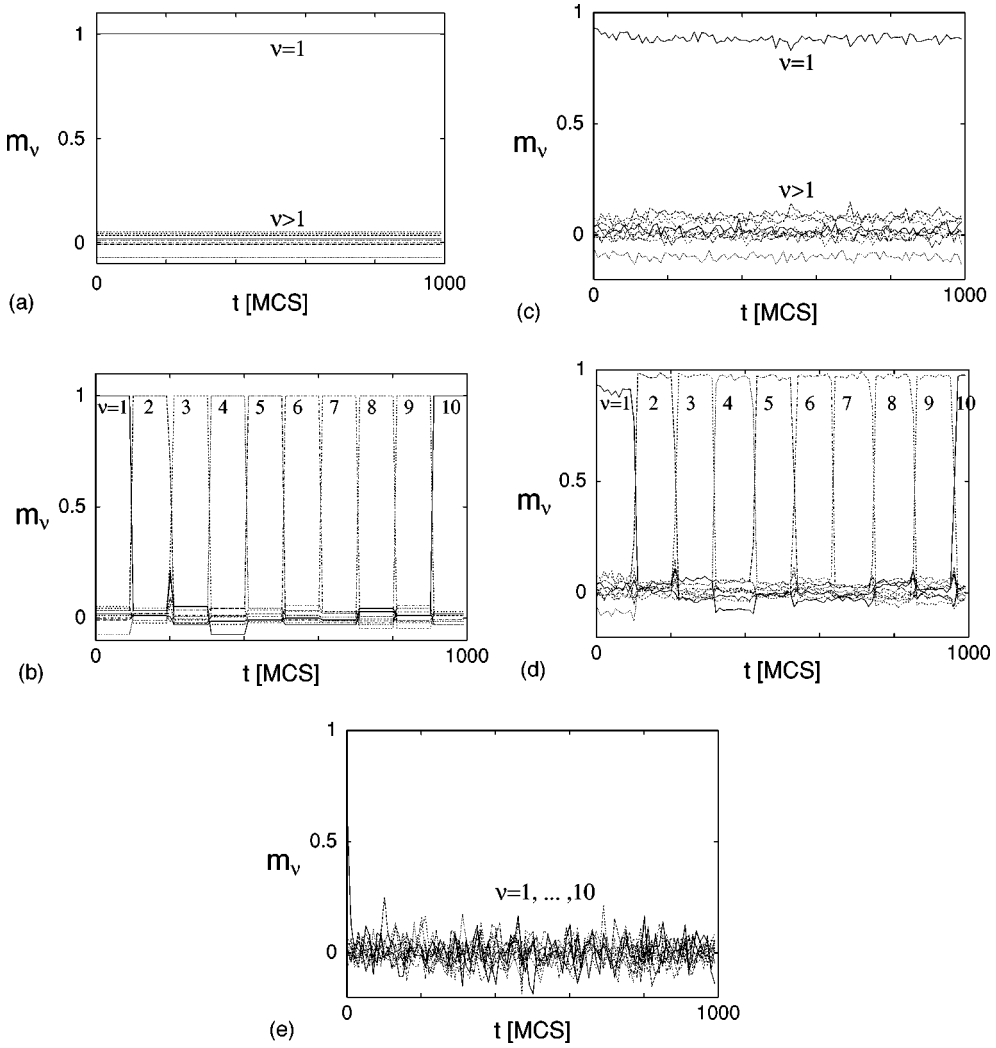

FIG. 1. Behavior of the overlap m_μ $(\mu=1,\ldots,p)$ in the asymmetric Hopfield model with the memory function $w(t)=\delta(t-\tau)$. The parameter values used in the simulations are $N=1000$, $p=10$, and (a) $T=0$, $\lambda=0.7$; (b) $T=0$, $\lambda=1.0$; (c) $T=0.3$, $\lambda=0.1$; (d) $T=0.3$, $\lambda=0.3$; (e) $T=0.7$, $\lambda=0.3$. Time t has been measured in units of the Monte Carlo steps per neuron (MCS) and the time delay τ set equal to 100 MCS.

however, random overlaps destroy the memory in the system. Thus the network, starting from the stationary-memory state at low temperatures, first makes a transition to the temporal-association state and then to the no-memory state, as the temperature is increased. Note that the two boundaries separating the temporal-association state from the stationary-memory one and from the no-memory one do not meet at $\lambda=0$. This leads to a narrow interval of T in which the network undergoes double transitions as λ is increased from zero, from the stationary-memory state to the no-memory one and subsequently to the temporal-association state. It is also of interest to observe the shift of the boundaries with the storage α: With increasing α, the stationary memory is suppressed at low temperatures, which reflects that fluctuations in the local fields tend to induce transitions between patterns. At high temperatures, on the other hand, large fluctuations tend to mix all the patterns and to give random overlaps, thus suppressing temporal association. Further, Fig. 2 shows how the storage capacity α_c changes with λ. Namely, the boundary at $T=0$ between the stationary-memory state and the temporal-association one, which gives the critical value λ_c for given α, can be considered to give the storage capacity α_c for given λ: $\alpha_c=0.1$, 0.05, 0.01, and 0.001 for $\lambda \approx 0.42$, 0.53, 0.78, and 0.95, respectively. In this way it is revealed that as λ is raised from zero, the storage capacity α_c decreases markedly from 0.138, the value in the symmetric network $(\lambda=0)$ [2].

Here the finite-size effects have been checked for each value of α, and systems of sizes which appear to display asymptotic behavior have been used in obtaining Fig. 2. The typical behavior of the system according to the system size is displayed in Fig. 3, for $\alpha=0.01$ and $N=500$, 1000, 2000, and 4000. It is observed that the system apparently reaches the asymptotic regime for $N=2000$. Even the system of size $N=1000$ already displays negligible finite-size effects except at very low temperatures.

III. ASYMMETRIC DYNAMIC MODEL

The dynamic model employs continuous-time dynamics, which is neither totally synchronous nor totally asynchronous, and is more realistic than the Hopfield models in view of the biological situation. At the price of this, however, the model lacks the Hamiltonian which governs the equilibrium

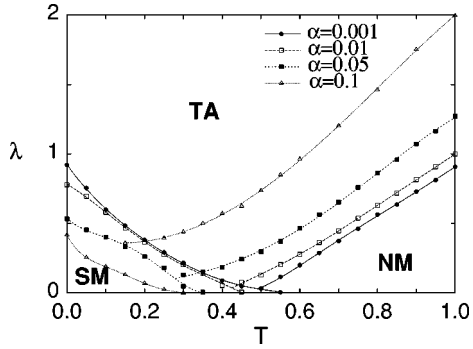

FIG. 2. Schematic phase boundaries of the asymmetric Hopfield model with noise for various values of the storage α. The size of the network is $N=10\,000$, 4000, 1000, and 1500 for $\alpha=0.001$, 0.01, 0.05, and 0.1, respectively. Each line represents the least-square fit of the corresponding data, the typical error bar of which is about the size of the symbol.

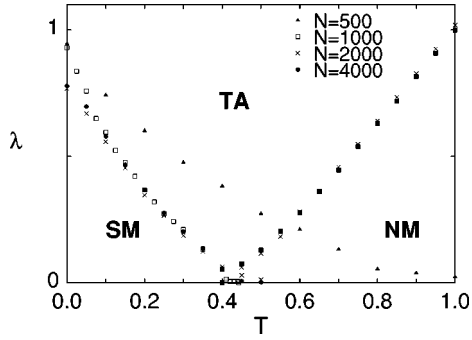

FIG. 3. Phase boundaries of the asymmetric Hopfield model for $\alpha=0.01$ and for $N=500$, 1000, 2000, and 4000. Even the system of size $N=1000$ already displays negligible finite-size effects except at very low temperatures.

state and, accordingly, the methods of equilibrium statistical mechanics are not applicable. Instead, the dynamic model of neural networks is described by the master equation for the joint probability $P(\{s_i\},t;\{s_i'\},t-\tau_d)$ that the system is in state $\{s_i'\}$ at time $t-\tau_d$ and in state $\{s_i\}$ at time t, where τ_d is the time delay in the signal propagation. The resulting master equation leads the evolution equations for physical quantities to assume the form of appropriate differential-difference equations [10]. For example, the activity of the kth neuron, $\sigma_k(t)\equiv\langle s_k\rangle_t\equiv\Sigma_{\{s_i\},\{s_i'\}}s_kP(\{s_i\},t;\{s_i'\},t-\tau_d)$, satisfies the equation

$$\frac{1}{b}\frac{d\sigma_k(t)}{dt}=\left(\frac{1}{2}-a\right)-\left(\frac{1}{2}+a\right)\sigma_k(t)+\frac{1}{2}\langle(1-s_k)\tanh\beta h_k(t-1)\rangle_t, \tag{5}$$

where a and b are the ratios of the refractory period to the action potential duration and of the delay time to the refractory period, respectively, and time t has been rescaled in units of the delay time τ_d.

The simple case of the symmetric couplings both at zero and at finite storages has been shown to display desirable features similar to those of the Hopfield model [10,12]: There exists the critical temperature $T_c(\alpha)$ depending on the storage α, below which there emerges macroscopic coherence between the network state and one of the embedded patterns. In particular, the storage capacity α_c for memory retrieval at zero temperature is given by that of the Hopfield model divided by $(1+a^2)$. The phase diagram drawn in the (T,a,α) space exhibits a variety of interesting behaviors, depending on the value of the parameters. For sufficiently small α and a less than 1/2, the network undergoes two successive transitions as the temperature is lowered, whereas for large α, only a single transition occurs regardless of the value of a. The case $a=1/2$ deserves particular attention since the memory capacity in this case takes its maximum value at zero temperature and the critical temperature for memory retrieval reaches the highest value at zero storage.

We now introduce the asymmetric Hebb rule, as in the preceding section:

$$J_{ij}=\frac{1}{N}\sum_{\mu=1}^{p}\xi_i^\mu\xi_j^\mu+\frac{\lambda}{N}\sum_{\mu=1}^{q}\xi_i^{\mu+1}\xi_j^\mu, \quad i\neq j, \tag{6}$$

where a cyclic sequence is again incorporated by setting $\xi_i^{q+1}=\xi_i^1$. We consider the case $q=p$, and make use of the mean-field approximation in Eq. (5), which is expected to be correct for the infinite-range interaction. Equation (5) then reads

$$\frac{1}{b}\frac{d\sigma_k(t)}{dt}=\left(\frac{1}{2}-a\right)-\left(\frac{1}{2}+a\right)\sigma_k(t)+\frac{1}{2}[1-\sigma_k(t)]\times\tanh\left\{\beta\sum_{\nu=1}^{p}[\xi_k^\nu m_\nu(t-1)+\lambda\xi_k^{\nu+1}m_\nu(t-\tilde{\tau})]\right\}, \tag{7}$$

where the *order parameter* $m_\nu(t)\equiv N^{-1}\Sigma_i\xi_i^\nu\sigma_i(t)$ describes the average overlap between the network and the νth embedded pattern, and $\tilde{\tau}$ denotes the time delay of the asymmetric coupling (relative to that of the symmetric one, τ_d). Multiplying Eq. (7) by $N^{-1}\xi_i^\mu$ and summing over i, we obtain the equation for the order parameter m_μ:

$$\frac{1}{b}\frac{dm_\mu(t)}{dt}=-\left(\frac{1}{2}+a\right)m_\mu(t)+\frac{1}{2N}\sum_i\xi_i^\mu[1-\sigma_i(t)]\times\tanh\left\{\beta\sum_{\nu=1}^{p}[\xi_i^\nu m_\nu(t-1)+\lambda\xi_i^{\nu+1}m_\nu(t-\tilde{\tau})]\right\}, \tag{8}$$

which, together with Eq. (7), governs the time evolution of the network.

It is obvious that Eq. (8) possesses the trivial solution $m_\mu(t)=0$ for all μ, corresponding to the disordered state, i.e., the state without memory. The stability of this trivial solution can easily be examined by linearizing the equation, and it turns out that the null solution is asymptotically stable at temperatures higher than $T_2\equiv 4a/(1+2a)^2$. Note that T_2

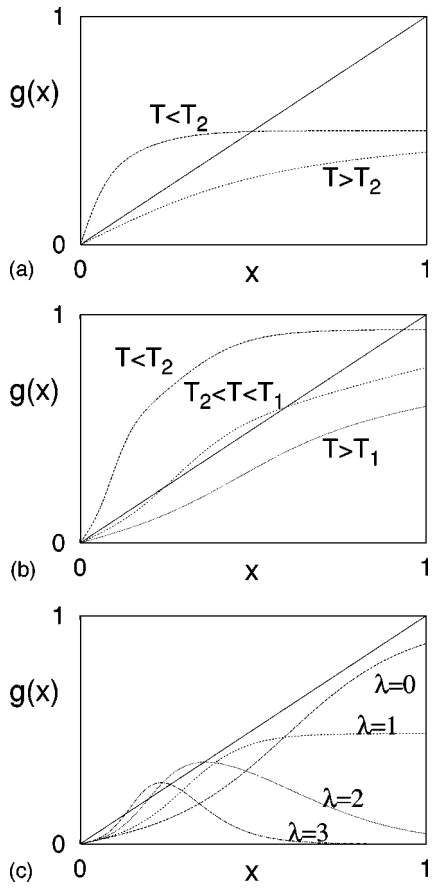

FIG. 4. Behavior of the function $g(x)$ for given λ, together with the straight line $y=x$, (a) for $a>a_c$ and (b) for $a<a_c$. The behavior at given temperature T between $T_1(\lambda=1)$ and $T_1(\lambda=2)$ is shown in (c) for various values of λ, indicating that T_1 is an increasing function of λ.

is independent of λ and in particular the same as the value for the symmetric coupling ($\lambda=0$) obtained in Ref. [10].

For $T<T_2$, on the other hand, Eqs. (7) and (8) allow nontrivial solutions. We investigate the Mattis solution which is fully correlated with just one of the learned patterns, i.e.,

$$m_\mu = m\,\delta_{\mu,1}. \tag{9}$$

In this Mattis solution m is given by the nonzero solution of

$$m=\frac{4a}{1+2a}\left\langle\!\left\langle \frac{\xi^1\tanh[\beta(\xi^1+\lambda\xi^2)m]}{1+2a+\tanh[\beta(\xi^1+\lambda\xi^2)m]}\right\rangle\!\right\rangle, \tag{10}$$

where $\langle\langle\cdots\rangle\rangle$ stands for the average taken with respect to the distribution of $\{\xi_i^\mu\}$. Here we have replaced the average over the neurons by that over the distribution of the memories: $N^{-1}\Sigma_i f(\xi_i)=\langle\langle f(\xi)\rangle\rangle$. This self-averaging property should be valid for $N\to\infty$ and fixed p, if the distribution of the patterns is essentially random. For simplicity, ξ_i^μ's are assumed to take the values $+1$ and -1 with equal probabilities. It is then straightforward to perform the average in Eq. (10), which yields

$$m=\frac{2a\tanh[\beta(1+\lambda)m]}{(1+2a)^2-\tanh^2[\beta(1+\lambda)m]} + \frac{2a\tanh[\beta(1-\lambda)m]}{(1+2a)^2-\tanh^2[\beta(1-\lambda)m]}\equiv g(m). \tag{11}$$

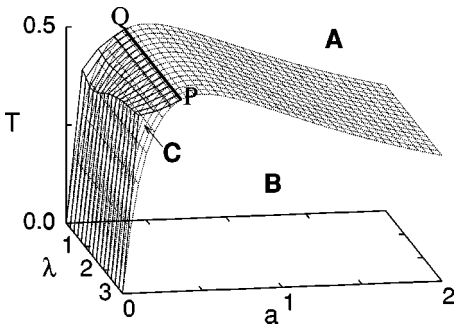

FIG. 5. Existence of the solution in the (T,a,λ) space. A, B, and C denote the regions of the null solution, the Mattis solution, and the mixed-state solution, respectively, whereas PQ represents the tricritical line.

Figure 4 shows two kinds of solution of Eq. (11) according to the value of a: (a) $a>a_c\equiv(\sqrt{3}-1)/2$ and (b) $a<a_c$. Here a_c is determined by the nonlinear equation $g''(0)=0$ and does not depend on λ. For $a>a_c$, the Mattis solution exists only at temperatures lower than T_2, and disappears continuously as the temperature T is raised to T_2. For $a<a_c$, the Mattis solution still exists at low temperatures ($T<T_2$); at intermediate temperatures ($T_2<T<T_1$), on the other hand, the null solution and the Mattis one coexist with different basins of attraction. As T is increased further, the average overlap m in general decreases and vanishes abruptly at $T=T_1$. Thus there appears a discontinuous transition at temperature T_1, which is determined by the coupled equations $g(x^*)=x^*$ and $g'(x^*)=1$. At given temperature the behavior of $g(x)$ for various values of λ is displayed in Fig. 4(c), which indicates that T_1 is an increasing function of λ. In particular, it is obvious that Fig. 4(c) exhibits the behavior at temperatures between $T_1(\lambda=1)$ and $T_1(\lambda=2)$. Accordingly, for $a<a_c$ the network is expected to exhibit successive transitions as T is lowered: a discontinuous transition at $T_1(\lambda)$ from the null state to the mixed state followed by a continuous transition at T_2 to the ordered state.

With varying λ, we have examined the basins of attraction, and obtain Fig. 5, which displays two surfaces, $T=T_2$ and $T=T_1$, meeting at the straight line $a=a_c$. Regions A above the two surfaces, B below the two, and C between the two correspond to the existence of the null solution, of the Mattis solution, and of the mixed state, respectively. Whereas region B is separated from A or from C via the continuous transition surface $T=T_2$, the boundary between A and C, existing only for $a<a_c$, constitutes the discontinuous transition surface $T=T_1$. In the limit $a\to0$, both surfaces approach the line $T=0$ but with different slopes. On

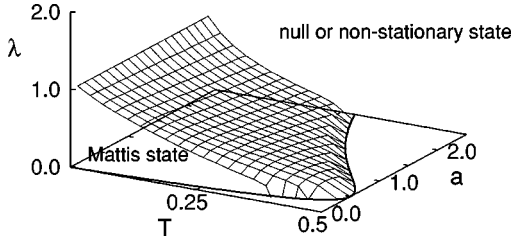

FIG. 6. Upper bound of the phase boundary separating the Mattis state in the (T,a,λ) space. The thick solid line on the $\lambda=0$ plane represents the continuous transition line T_2.

line PQ, which is given by $a=a_c$ and $T=4a_c/(1+2a_c)^2$, the two surfaces meet. Accordingly, PQ may be regarded as a tricritical line.

Note that these solutions existing in various regions do not necessarily correspond to the physical solutions since their stability is not guaranteed. It is known that they are in general stable in the absence of the asymmetric coupling $(\lambda=0)$ [10]. To examine the stability of the Mattis solution in the presence of the asymmetric coupling $(\lambda\neq 0)$, we consider a small deviation from the Mattis solution in regions B and C and put $m_\mu(t)=m_\mu+\delta m_\mu(t)$ [and correspondingly, $\sigma_i(t)=\sigma_i+\delta\sigma_i(t)$]. Substituting into Eqs. (7) and (8), together with $\delta m_\mu \sim e^{\gamma_\mu t}$, leads to the stability determined by the exponent γ_μ. Here the stable Mattis solution should be accompanied by the exponents γ_μ with negative real parts for all $\mu=1,\ldots,p$. However, the resulting p coupled differential-difference equations are too complicated to allow general analysis. We thus consider the simple case $\gamma_\mu=\gamma$, and compute the surface confining the region where the overlap m is finite and γ has a negative real part in the long time limit.

The obtained boundary surface in the (T,a,λ) space is displayed in Fig. 6. In the symmetric case $(\lambda=0)$, the stability boundary is expected to coincide with the transition line T_2 [10]. Figure 6 shows that the stability boundary for $\lambda=0$, given by the locus of the surface on the T-a plane, indeed agrees well with the continuous transition line T_2 represented by the thick solid line. For general values of λ, on the other hand, it should be noted that due to the restriction $\gamma_\mu=\gamma$, the obtained boundary in Fig. 6 comprises an upper bound for the true phase boundary. We thus regard Fig. 6 as the approximate phase diagram for the Mattis state in the (T,a,λ) space. Nevertheless it shows clearly that as λ increases, the Mattis state becomes unstable and replaced by the disordered state or by the nonstationary state.

The above analytic investigation is limited to the equilibrium (fixed-point) behavior in the thermodynamic limit with finite p. Unlike the symmetric network, however, the asymmetric one is expected to exhibit a variety of dynamics which may not be obtained via the analytic (equilibrium) analysis. In addition, the zero-storage limit $\alpha\equiv p/N\to 0$ is far from practical in real networks of finite sizes. To investigate the dynamic behavior of the asymmetric network with finite storage capacity, we thus resort to numerical methods and perform simulations of the coupled differential-difference equations (7) and (8). The solutions of the coupled equations and the corresponding phases are investigated for various values of the parameters, T, λ, and a, while for convenience b is set equal to unity. The relative time delay $\tilde{\tau}$ is observed not to affect the asymptotic behavior and set equal to unity throughout the simulations. Figure 7 displays the typical behaviors of the average overlaps in the system starting from the initial pattern $\xi^{\nu=1}$: Here the transition from the stationary-memory state at low T and for small λ [shown in (a)] to either the temporal-association state [shown in (b)] upon increasing λ or to the no-memory state [shown in (c)] upon raising T can be observed. It is of interest that the average overlap in the no-memory state decays to zero as shown in (c); this is in contrast with the asymmetric Hopfield model, displaying large fluctuations.

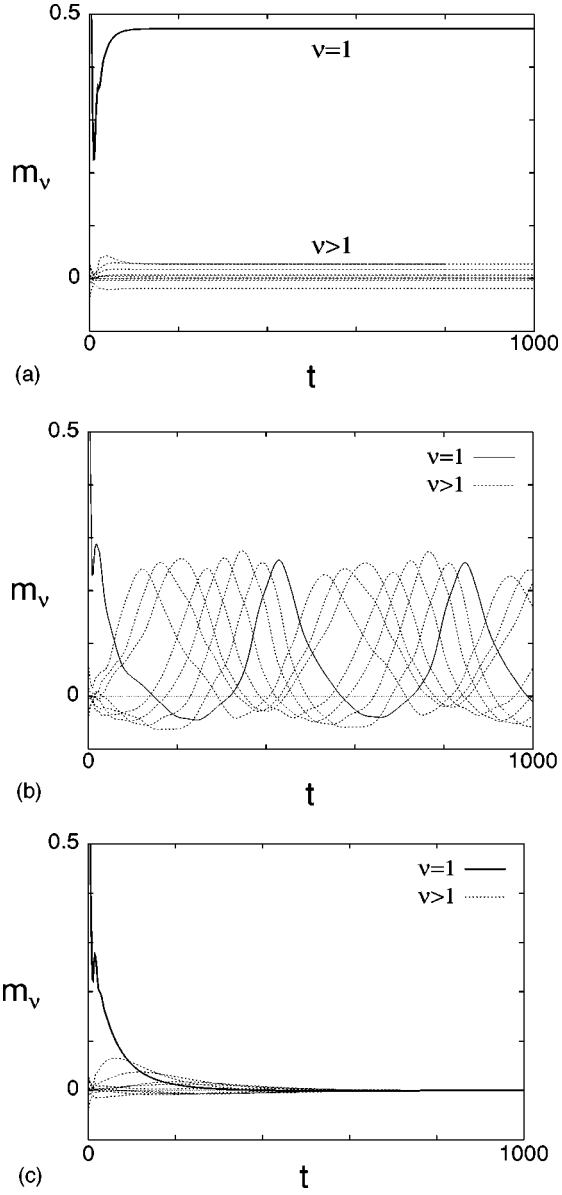

FIG. 7. Behavior of the overlap m^μ $(\mu=1,\ldots,p)$ in the asymmetric dynamic model for the parameters $N=1000$, $p=10$, and (a) $T=0.2$, $\lambda=0.2$; (b) $T=0.2$, $\lambda=0.8$; (c) $T=0.6$, $\lambda=0.2$. Time t has been measured in units of one-tenth of the delay time, $0.1\tau_d$.

In order to describe the ability of the asymmetric dynamic model to recall a learned pattern or a full cycle, we have performed extensive simulations and obtained the complete phase diagrams for various values of α, which are displayed in Fig. 8. Each phase diagram consists of two surfaces in the

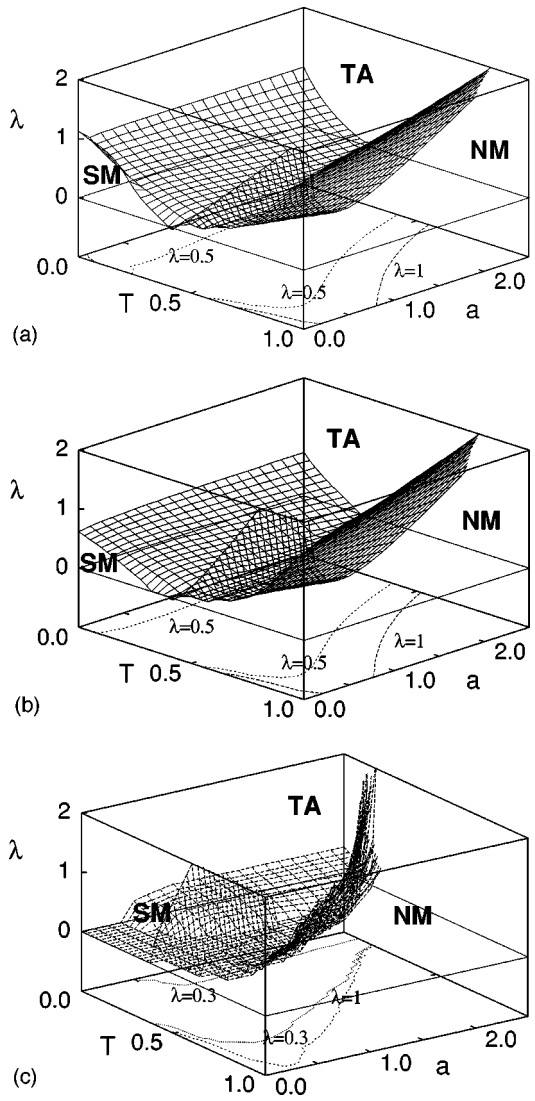

FIG. 8. Phase diagram of the asymmetric dynamic model in the (T,a,λ) space, for (a) $\alpha=0.001$, $N=5000$; (b) $\alpha=0.01$, $N=2000$; (c) $\alpha=0.05$, $N=600$. The dashed lines on the bottom plane represent the contours of constant λ.

(T,a,λ) space: one separating the stationary-memory (SA) state and the other the no-memory (NM) state from the temporal-association (TA) state, respectively. Here the system has been considered to be in the stationary-memory state and in the no-memory state if $m_\mu > \Sigma_{\nu\neq\mu} m_\nu$ for a single memory μ and if $m_\nu = O(N^{-1/2})$ for all $\nu = 1,2,\ldots,p$, respectively. As in the asymmetric Hopfield model, there also exists a very narrow interval of T in which the system undergoes double transitions as λ is increased from zero, from the stationary-memory state to the no-memory one and subsequently to the temporal-association state, although the no-memory state occupies only a tiny region of small λ just above zero and cannot be observed clearly in Fig. 8. Figure 8 shows that the contours of constant λ represented by the dashed lines on the bottom plane lead to the maximum values of T around $a=1/2$. Accordingly, the optimal memory capability is reached when the refractory period and the action potential duration are of the same order, regardless of the strength of the asymmetric coupling. It can also be observed that the region of the stationary-memory state shrinks

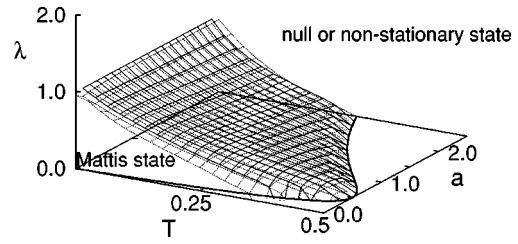

FIG. 9. Comparison of the analytic results obtained in the limit $\alpha\to 0$ (solid-line surface) and simulations performed for $\alpha=0.002$ (dotted-line surface). The thick solid line on the $\lambda=0$ plane again represents the continuous phase-transition boundary.

with the storage α, which plays a role similar to that of the temperature T. While for small α the temporal association becomes optimal around the temperature T_2 [see (a) and (b)], (c) reveals the drastic deterioration of the memory capability as α is increased toward the storage capacity α_c [$<\alpha_c(\lambda=0)\approx 0.138/(1+a^2)$].

The simulation result for $\alpha=0.002$ and the analytic one $(\alpha\to 0)$ are compared in Fig. 9, which shows good agreement with each other except for small a and high T. Since the analytic result gives only an upper bound for the precise phase diagram in the limit $\alpha\to 0$, the true boundary of the Mattis state for $\alpha=0$ is expected to be located between the two surfaces in Fig. 9.

IV. SUMMARY

The characteristics of temporal association in neural networks have been investigated both analytically and numerically, with emphasis on the effects of finite storage and temperatures. We have first considered the asymmetric Hopfield model in the presence of noise, and presented several simulation results. The phase diagram has been obtained in the plane of the temperature and the degree of asymmetry, for various storage values. We have then turned to the dynamic model, which has also been made capable of temporal association by introducing asymmetric couplings in a similar way to the Hopfield model. In the dynamic model, the ratio a of the refractory period to the action potential duration is a relevant parameter, in addition to the temperature and the degree of asymmetry, and the phase diagram in the corresponding three-dimensional parameter space has been obtained via stability analysis in the zero storage limit. We have further performed extensive numerical simulations, which have yielded the phase diagram for various (nonzero) storage values. It has been observed that the memory capability of the network reaches its maximum around $a=1/2$, regardless of the storage or the strength of the asymmetric coupling. It is of interest to note that the refractory period and the action potential duration are indeed comparable to each other in the real biological system, which is optimal according to our results.

ACKNOWLEDGMENTS

This work was supported in part by the Basic Science Research Institute Program, Ministry of Education of Korea, and in part by the Korea Science and Engineering Foundation through the SRC program.

[1] J. J. Hopfield, Proc. Natl. Acad. Sci. USA **79**, 2554 (1982); W. A. Little and G. L. Shaw, Math. Biosci. **39**, 281 (1978).
[2] D. J. Amit, H. Gutfreund, and H. Sompolinsky, Phys. Rev. Lett. **55**, 1530 (1985); Phys. Rev. A **32**, 1007 (1985).
[3] P. Peretto, *An Introduction to the Modeling of Neural Networks* (Cambridge Univ. Press, Cambridge, 1992); *Models of Neural Networks II*, edited by E. Domany, J. L. van Hemmen, and K. Schulten (Springer-Verlag, New York, 1994); *Neural Networks: The Statistical Mechanics Perspective*, edited by J.-H. Oh, C. Kwon, and S. Cho (World Scientific, Singapore, 1995).
[4] H. Sompolinsky and I. Kanter, Phys. Rev. Lett. **57**, 2861 (1986).
[5] H. Gutfreund and M. Mezard, Phys. Rev. Lett. **61**, 235 (1988).
[6] U. Riedel, R. Kühn, and J. L. van Hemmen, Phys. Rev. A **38**, 1105 (1988).
[7] P. Spitzner and W. Kinzel, Z. Phys. B **74**, 539 (1989).
[8] A. C. C. Coolen and T. W. Ruijgrok, Phys. Rev. A **38**, 4253 (1988); D. Horn and M. Usher, *ibid.* **40**, 1036 (1989); H. Nishimori, T. Nakamura, and M. Shiino, *ibid.* **41**, 3346 (1990).
[9] A. V. M. Herz, Z. Li, and J. L. van Hemmen, Phys. Rev. Lett. **66**, 1370 (1991); K. Bauer and U. Krey, Z. Phys. B **84**, 131 (1991).
[10] M. Y. Choi, Phys. Rev. Lett. **61**, 2809 (1988).
[11] Note that at zero storage ($\alpha=0$) the critical value λ_c is equal to unity.
[12] G. M. Shim, M. Y. Choi, and D. Kim, Phys. Rev. A **43**, 1079 (1991).